

---

Oral presentation | Turbulence simulation (DNS,LES,RANS)

## Turbulence simulation(DNS,LES,RANS)-IV

Thu. Jul 18, 2024 2:00 PM - 4:00 PM Room B

---

### [11-B-04] Investigation of Filter Stability and Consistency for High-Resolution Turbulent Flow Simulations on Finite-Domains

\*James Coder<sup>1</sup> (1. Penn State University)

Keywords: Turbulence, Filtering, High-order methods

# Investigation of Filter Stability and Consistency for High-Resolution Turbulent Flow Simulations on Finite-Domains

James G. Coder\*

Corresponding author: jcoder@psu.edu

\* Pennsylvania State University, USA

**Abstract:** The mathematical and practical behavior of finite-domain filters is explored for applications to turbulent flow simulations. High-order filters are constructed for finite-difference schemes that satisfy summation-by-parts, with calibration that considers the spectral behavior at boundaries and the integration norm of the numerical scheme, leading to both symmetric and asymmetric filters. All filters studied are contractive, but additional analysis of potential transient growth behavior is performed. The filters are applied to the one-dimensional linear advection equation and the inviscid evolution of two-dimensional, incompressible turbulence. It is observed that symmetric filters offer better overall performance with provable stability properties, but the performance of asymmetric filters for turbulence simulations was still acceptable.

*Keywords:* Turbulence, Filtering, High-order methods, energy stability

## 1 Introduction

Numerical schemes with high resolution and low dissipation are the cornerstone of scale-resolving turbulent flow simulations. For flows without shockwaves, high-order-accurate central-difference operators are frequently used. Such operators may be either explicitly defined or Padé-type compact difference schemes [1, 2]. However, conventional central-difference schemes do not have any natural dissipation, and as such, they are prone to odd-even decoupling that can (and do) destabilize simulations of non-linear conservation laws such as the Navier-Stokes equations. One possible remedy is to employ either artificial dissipation, which acts like upwinding by penalizing the formation of oscillations without harming the formal order of accuracy [3, 4, 5]. Similarly, one could use adaptive schemes such as the WENO class of schemes which automatically adapt the stencil based on local solution smoothness [6]. Another possibility is to use high-order filters that directly remove high-wavenumber oscillations from the solution and mimic the effect of a sub-grid-scale turbulence model. Such approaches are commonly known as implicit large-eddy simulations (ILES), and the role of the filter is illustrated below in Fig. 1 (originally from Garmann[7]). When one considers the modified wavenumber behavior of the underlying finite-difference scheme, it is evident that high-wavenumber content is poorly resolved by the scheme, as the magnitude of the derivatives can be significantly mis-predicted. Nominally, the filter inhibits the ability of underresolved content to contaminate the solution.

In typical practice, filter formulae are constructed based on Taylor-series analysis. They feature an integration norm (also known as a mass matrix), and add/subtract a portion of even derivative of the solution (the exact operation depends on the order of the derivative). The calibration of the even-derivative term is based on Fourier analysis such that the so-called  $\pi^{\text{th}}$  mode, i.e.  $k\Delta x = \pi$  where  $k$  is the dimensional wavenumber, is removed as the Nyquist wavenumber of the signal; however, this behavior is guaranteed only on infinite/periodic domains.

Implementation of these filters on finite domains requires biased boundary closure formulae, which are also constructed based on Taylor analysis and calibrated using Fourier analysis, tacitly assuming an infinite domain. The combination of interior and boundary filters can have unintended consequences on finite domains. For example, the biased boundary formula introduce overshoots that promote an increase of energy at low-to-moderate wavenumbers. In the context of implicit large-eddy simulations, this is a form of backscatter and is generally regarded as undesirable since solution content at those wavenumbers is already well-resolved by the scheme. Another potential problem on finite domains is non-symmetry in the filter operator, which leads to non-orthogonal eigenvectors and a possibility of non-modal growth of

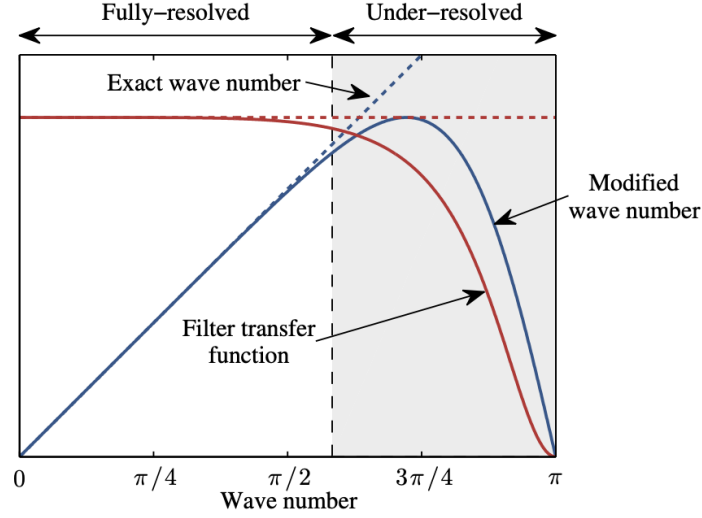


Figure 1: Schematic of the role of a filter as a sub-grid-scale model for implicit large-eddy simulations (from Ref. [7]).

solution content (commonly known as transient growth [8]), even though the magnitude of all eigenvalues are less than or equal to one.

The primary objective of this paper is to explore the mathematical and practical behavior of finite-domain filters for applications to turbulent flow simulations. Focus is given to finite-difference schemes that satisfy the summation-by-parts convention, with both diagonal and multi-diagonal norms. Bespoke high-order filters are constructed for the schemes, with calibration that considers the spectral behavior at boundaries and the integration norm of the numerical scheme. All filters considered will be contractive, i.e., their eigenvalue spectra will all be  $0 \leq \lambda \leq 1$ ; however, additional analysis of the transient growth will be performed using singular value decompositions. The filters (and underlying schemes) will be applied to multiple test cases to evaluate the behaviors in a practical sense.

## 2 Analysis Methodology

### 2.1 Fourier Transforms

The standard technique for analyzing the behavior of a filter is to consider the spectral transfer function. That is, one considers the Fourier transforms of both the filtered and unfiltered quantities, e.g.,

$$u(x) = \sum_{k=0}^{\infty} U_k e^{ikx} \quad (1)$$

where  $i$  is the imaginary unit. Although properly defined on an infinite/periodic domain, it is nonetheless insightful on finite domains. Accordingly, the transfer function in wavenumber space for point  $j$  in the domain may be defined as

$$\mathcal{G}_j(k\Delta x) = \frac{\hat{U}_k}{U_k} \Big|_j = \sum_l a_{jl} e^{ik\Delta x(l-j)} \quad (2)$$

where  $a_{jl}$  are the entries of the filter matrix  $\mathcal{F}$  and  $k\Delta x = [0, \pi]$ . In this expression,  $k$  the dimensional wavenumber with its upper limit being the Nyquist wavenumber for the  $\Delta x$  of the domain.

### 2.2 Eigenvalue Analysis

In the limit of infinite domains or the special case of periodicity, the spectral transfer function is exactly equivalent to the eigenvalue spectrum of the filter matrix. On a finite, non-periodic domain, however, these are no longer equivalent and preference should be given to the discrete eigenvalue decomposition, i.e.

$$\mathcal{F} = T\Lambda T^{-1} \quad (3)$$

where  $T$  contains the eigenvectors and  $\Lambda$  the eigenvalues  $\lambda_j$ . The eigenvectors of  $\mathcal{F}$  form a complete basis, so any input signal may be represented as a linear combination of the eigenvectors. So long as all eigenvalues are real and  $0 \leq \lambda_j \leq 1$ , the filter is deemed to be contractive and repeated application will not result in continuous growth of content.

### 2.3 Singular Value Decompositions

General filters of interest are not guaranteed to be symmetric with respect to the mass matrix  $\mathcal{P}_f$ . Therefore, the set of eigenvectors will be non-orthogonal. While the eigenspectrum may be contractive, non-orthogonality of the eigenvectors allows the possibility of a transient growth phenomenon to occur. This behavior is illustrated in Fig. 2, in which the vector  $\mathbf{w} = \mathbf{v}_1 + \mathbf{v}_2$ . Although the contribution of  $\mathbf{v}_2$  decreases from  $n$  to  $n+1$  and the contribution of  $\mathbf{v}_1$  remains constant, reflecting an associated eigenvalues being less than or equal to one, the overall magnitude of  $\mathbf{w}$  increases.

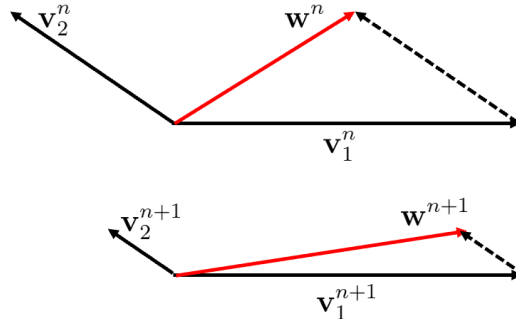


Figure 2: Transient growth phenomenon due to non-orthogonal vectors.

The transient growth induced by a filter matrix can be found by considering the weighted norms of the input and output vectors. A generalized discrete norm takes the form,

$$\|\mathbf{a}\|_{\mathcal{M}}^2 = \mathbf{a}^T \mathcal{M} \mathbf{a} \quad (4)$$

where  $\mathcal{M}$  is a symmetric positive definite weighting matrix. It then follows that

$$\frac{\|\hat{\mathbf{u}}\|_{\mathcal{M}}^2}{\|\mathbf{u}\|_{\mathcal{M}}^2} = \frac{\mathbf{u}^T \mathcal{F}^T \mathcal{M} \mathcal{F} \mathbf{u}}{\mathbf{u}^T \mathcal{M} \mathbf{u}} \quad (5)$$

Thus, the optimum growth of the vector magnitude is then found by taking the singular value decomposition of  $\mathcal{R} \mathcal{F} \mathcal{R}^{-1}$  where  $\mathcal{M} = \mathcal{R}^T \mathcal{R}$  is found using a Cholesky decomposition.

The choice of the weighting matrix  $\mathcal{M}$  can be subjective for different applications. Choosing the identity matrix returns an  $L^2$ -norm that may be interpreted as the energy of the solution vector. Volumetric weighting may be used if available, as could the mass matrices of the associated numerical scheme if they are symmetric positive definite.

## 3 Brief Overview of High-Order Filters

The general form of the high-order filters considered in this work is,

$$\mathcal{P}_f \hat{\mathbf{u}} = [\mathcal{P}_f - \mathbf{C} \Delta x^{2n} \mathcal{D}_{2n}] \mathbf{u} = \mathcal{P}_f \mathcal{F} \mathbf{u} \quad (6)$$

In this expression,  $\hat{\mathbf{u}}$  is the filtered value of  $\mathbf{u}$ ,  $\mathcal{P}_f$  is a suitable integration norm,  $\mathcal{D}_{2n}$  is an even-order derivative operator, and  $\mathbf{C}$  is a diagonal matrix of weights usually chosen based on Fourier analysis of the filter stencil.

The form of Eq. 6 can be extended to include additional even-order derivative operators on the left- or right-hand sides; however, these have the effect of either lowering the formal accuracy of the filter and/or significantly increase the filter's computational cost.



This definition  $\mathcal{D}_{2n}$  is not necessarily unique, but it is convenient. With these definitions and appropriate constraints on the entries of  $\mathcal{P}_f$ , the filter is contractive with guaranteed stability in the  $\mathcal{P}_f$ -norm. On the interior of the domain, the entries of the  $\mathbf{C}$  matrix takes on the value,

$$C = \frac{1}{4^n} \quad (13)$$

Note that the values will always be positive in this specific formulation since the manner by which  $\mathcal{D}_{2n}$  is constructed guarantees positive entries on the main diagonal for all  $n$ .

Near the boundaries, the entries of  $\mathbf{C}$  and/or  $\mathcal{P}_f$  can be adjusted to provide desired characteristics. For example, Lundquist and Nordström [9] offer for the 8<sup>th</sup>-order filter

$$\mathcal{P}_f = \text{diag} \left( \frac{1}{16}, \frac{5}{16}, \frac{11}{16}, \frac{15}{16}, 1, \dots, 1, \frac{15}{16}, \frac{11}{16}, \frac{5}{16}, \frac{1}{16} \right) \quad (14)$$

which, by Fourier analysis with  $\mathbf{C} = \frac{1}{256}\mathbf{I}$ , removes the  $\pi^{\text{th}}$  mode at all points in the domain. It should be noted that such a mass matrix, as written, is neither conservative nor consistent; however, its diagonal nature can allow one or both qualities to be rectified by scaling entries of the  $\mathbf{C}$  matrix.

### 3.3 Padé Filters

Improved spectral support of the filter (i.e., a higher roll-off wavenumber) can be obtained through the use of a tri- and pentadiagonal mass matrix  $\mathcal{P}_f$  to create a Padé-like transfer function. Such filters are often used in tandem with Padé compact finite differencing, which already have improved spectral support and offer the existing machinery for evaluating such a filter. Thus, it is not uncommon for the bandwidth of  $\mathcal{P}_f$  to be the same as the underlying differencing scheme.

One notable, practical example of Padé-type filters is the Visbal-Gaitonde filter [2]. For interior points, the filter is structured as

$$\alpha_f \hat{u}_{j-1} + \hat{u}_j + \alpha_f \hat{u}_{j+1} = \alpha_f u_{j-1} + u_j + \alpha_f u_{j+1} - C(1 - 2\alpha_f) \Delta x^{2n} \mathcal{D}_{2n} u_j \quad (15)$$

Treatment of the boundary points is done by reverting to lower-order derivatives and biased stencils calibrated to remove the  $\pi^{\text{th}}$  oscillatory mode. This filter is used within the well-known FDL3DI solver [2], which employs a 6<sup>th</sup>-order compact differencing scheme with tridiagonal norm with an 8<sup>th</sup>-order interior filter. The value of  $\alpha_f$  is a user-specified parameter satisfying  $-1/2 < \alpha_f < 1/2$ . In the special case of  $\alpha_f = 0$ , the filter reverts to an explicit filter of order  $2n$ . The value of  $\alpha_f$  also need not be constant in the domain, and is often modified at the boundary to improve numerical behavior. It is important to note, however, that the mass matrix of the Visbal-Gaitonde filter generally does not match that of the underlying differencing scheme, nor is it a symmetric positive definite matrix. Thus while the Visbal-Gaitonde filter is demonstrably contractive, it lacks provable stability properties in the general case.

An alternative method for constructing Padé filters is to use an analogy to the Lundquist-Nordström filters. In this sense, the differencing operator  $\mathcal{D}_{2n}$  is built using Eq. 9. However, this makes the boundary stencils fully prescriptive rather than allowing a mix-and-match approach based on desired spectral properties.

To help provide provable stability properties, it is of interest to restrict the filter mass matrix to be consistent with that of the differencing scheme. For the Visbal-Gaitonde filter, this implies reducing  $\alpha_f$  to 1/3 rather than the more typical values in the range of 0.40-0.45. Another combination of interest is the bandwidth-optimized, pentadiagonal-norm summation-by-parts Padé scheme proposed by Coder [11]. The consistent interior filter stencil takes the form

$$\begin{aligned} -\frac{5}{128} \hat{u}_{j-2} + \frac{5}{32} \hat{u}_{j-1} + \frac{49}{64} \hat{u}_j + \frac{5}{32} \hat{u}_{j+1} - \frac{5}{128} \hat{u}_{j+2} &= -\frac{5}{128} u_{j-2} + \frac{5}{32} u_{j-1} + \frac{49}{64} u_j + \frac{5}{32} u_{j+1} - \frac{5}{128} u_{j+2} \\ &+ \frac{3}{8} \left( \frac{-u_{j-4} + 8u_{j-3} - 28u_{j-2} + 56u_{j-1} - 70u_j + 56u_{j+1} - 28u_{j+2} + 8u_{j+3} - u_{j+4}}{256} \right) \end{aligned} \quad (16)$$

A comparison of the 8<sup>th</sup>-order tridiagonal-norm Visbal-Gaitonde filter interior transfer function for various  $\alpha_f$  and the pentadiagonal norm filter are shown below in Fig. 3. Reducing  $\alpha_f$  decreases the effective

rolloff number of the filter, and the pentadiagonal norm provides a similar transfer function to the tridiagonal-norm filter with  $\alpha_f = 1/3$ . In all cases, the Padé-type filter provides increased wavenumber support compared to an explicit filter of the same order.

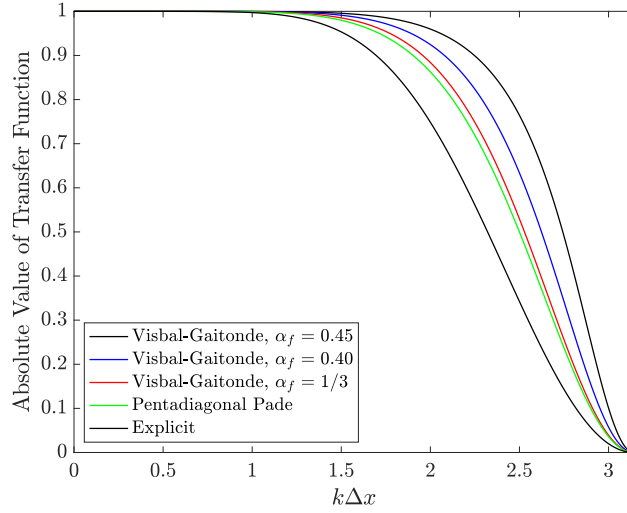


Figure 3: Comparison of interior stencil transfer function for various Padé filters.

### 3.4 Treatment of Boundary Points

An question for filter application is whether or not points on the boundary should be included in the filtering operation. The practical answer arises from how boundary conditions are imposed. For codes that rigidly specify the boundary condition at the boundary node, it is sensible to exclude this point from the filtering process. Take, for instance, imposing zero velocity at a no-slip boundary. Filtering that point could introduce a non-zero velocity there, violating the boundary condition. Re-imposing the boundary condition after filtering then may serve as a noise generator into the domain. Excluding the point in an explicit filter is straightforward and does not affect the rest of the domain. With an implicit, Padé-type filter, the global coupling of the mass matrix introduces an interaction between the boundary and interior stencils. Hence, the  $\pi^{\text{th}}$  mode might persist on the domain interior even though the stencils were calibrated to fully remove it. This is illustrated below in Fig. 4, which shows how the unfiltered boundary affects the response of the Visbal-Gaitonde filter with  $\alpha_f = 0.45$  [2].

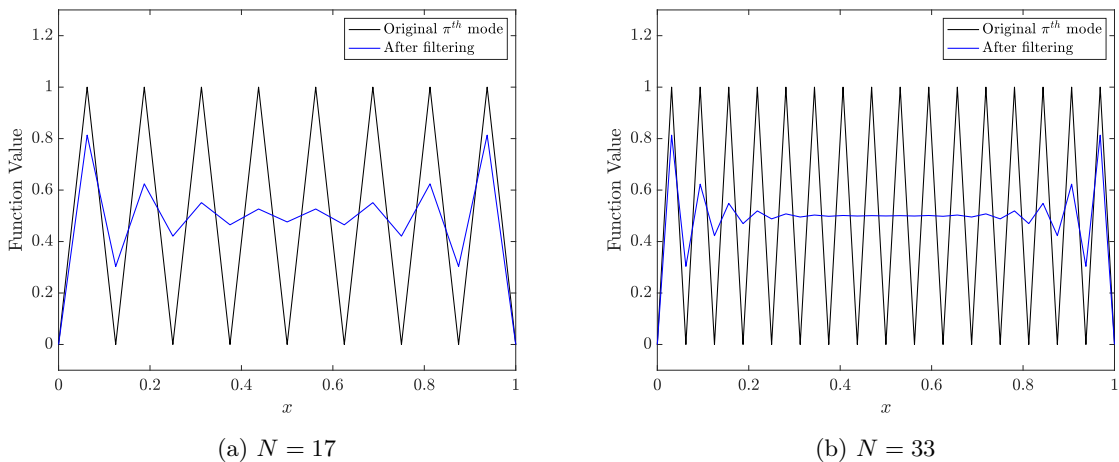


Figure 4: Effect of domain size on  $\pi^{\text{th}}$ -mode response of Visbal-Gaitonde filter with  $\alpha_f = 0.45$ .

Alternatively, codes that use penalty fluxes or simultaneous approximation terms permit the boundary node to not be exactly equal to the desired boundary condition. In such cases, there is no intrinsic

advantage to exactly preserving the boundary node at the expense of other advantageous filter properties or interior domain behavior. Since the entire domain is filtered, smoothness is maintained, and the penalty term at the boundary coerces the solution to satisfy the boundary conditions.

Focus in the subsequent analyses is restricted to filters that include the boundary point and work with differencing schemes that fall within the SBP-SAT paradigm. Furthermore, 8<sup>th</sup>-order filters will be used as representative examples of their respective types.

## 4 Analysis

### 4.1 Removing the $\pi^{\text{th}}$ Mode at Boundaries

Constructing a filter to remove the  $\pi^{\text{th}}$  mode near domain boundaries is widely assumed to be desirable, but it requires deeper inspection. Consider the behavior of 8<sup>th</sup>-order Lundquist-Nordström filter with  $\pi^{\text{th}}$ -mode removal as described above. The resulting transfer functions at the boundary points is shown in Fig. 5. There is a distinct penalty incurred in that overshoots in the transfer function become substantially larger. This is unavoidable with the boundary formulae and the goal of removing the  $\pi^{\text{th}}$  mode. Because it is an explicit formulation, these behaviors are independent of domain size.

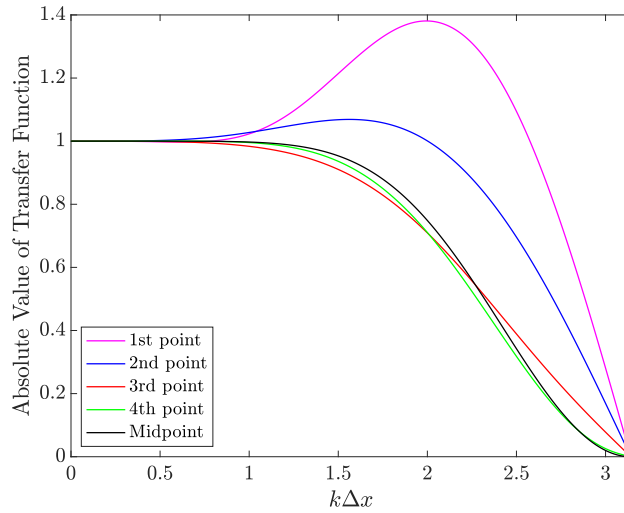


Figure 5: Lundquist-Nordström filter boundary transfer function with  $\mathcal{P}_f$  chosen to remove  $\pi^{\text{th}}$  mode.

Per Lundquist and Norström, the filter matrix is contractive with all eigenvalues being positive and  $0 \leq \lambda \leq 1$ . The filter is symmetric with respect to the provided definition of  $\mathcal{P}_f$  and thus the spectrum of singular values is equal to the eigenspectrum. Since the leading singular value is unity, no transient growth would occur against that norm. Unfortunately, this mass matrix is non-conservative and is thus inconsistent for use with any conservative differencing scheme. If one uses, say, the mass matrix of a standard 4<sup>th</sup>-order SBP differencing scheme with,

$$\mathcal{P} = \text{diag} \left( \frac{17}{48}, \frac{59}{48}, \frac{43}{48}, \frac{49}{48}, 1, \dots, 1, \frac{49}{48}, \frac{43}{48}, \frac{59}{48}, \frac{17}{48} \right) \quad (17)$$

the leading singular value of  $\mathcal{R}\mathcal{F}\mathcal{R}^{-1}$  where  $\mathcal{P} = \mathcal{R}^T\mathcal{R}$  is found to be  $\sigma_1 = 1.05849971$  for a domain with  $N = 9$  and asymptotes to  $\sigma_1 = 1.05504612$  for large  $N$ . The associated right singular vector for  $N = 33$  is plotted in Fig. 6. In other words, any content in the domain with this mode shape will grow by 5-6% with each application of the filter. It is evident from this filter (and, practically speaking, all filters of the general form considered in this work) that damping the  $\pi^{\text{th}}$  mode at boundaries will lead to asymmetry of the filter matrix with respect to a conservative  $\mathcal{P}$  norm (note that conservatism is a weaker test than consistency) and can be assumed to induce transient growth. Therefore, any filter that is consistent and symmetric cannot be expected to remove the  $\pi^{\text{th}}$  mode at the boundaries. This is not necessarily problematic, however. Asserting the presence of a  $\pi^{\text{th}}$  mode at the boundaries implicitly assumes the validity of a Fourier expansion in this region, which is inherently contradictory. Rather, it

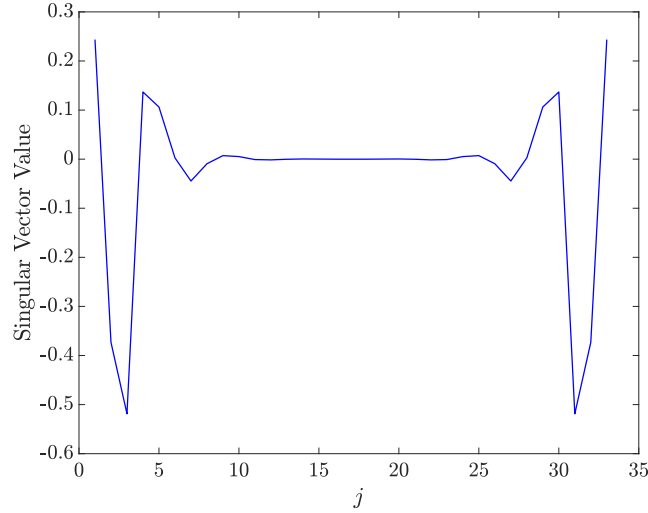


Figure 6: Leading right singular vector for  $N = 33$ .

is more appropriate to think in terms of the finite matrix properties than in terms of Fourier spectral response. Redefining  $\mathcal{P}_f$  to be consistent with the aforementioned 4<sup>th</sup>-order SBP scheme yields the boundary response shown in Fig. 7. While the  $\pi^{\text{th}}$  mode isn't removed, the overshoots are substantially reduced, and the symmetry of  $\mathcal{R}\mathcal{F}\mathcal{R}^{-1}$  keeps the leading singular value exactly at 1, thereby precluding any transient growth.

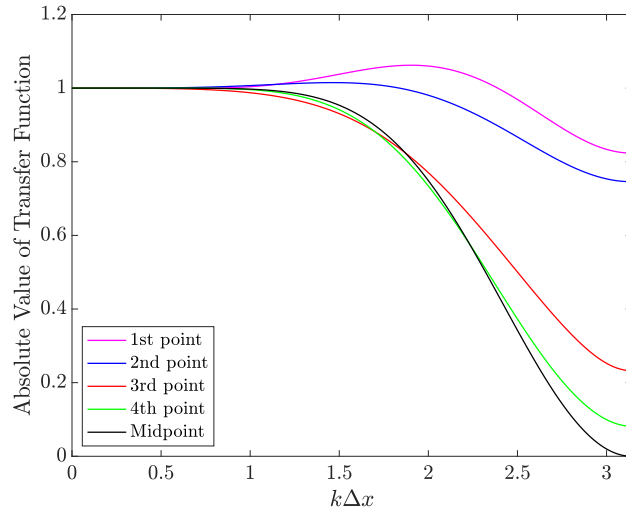


Figure 7: Lundquist-Nordström filter boundary transfer functions with consistent  $\mathcal{P}_f$ .

Similar general behaviors are observed with Padé-type filters. Here, a tridiagonal  $\mathcal{P}_f$  with cascade-norm boundary closure [12] is used based on a 6<sup>th</sup>-order finite-difference scheme. The boundary behaviors for  $N = 33$  are plotted in Fig. 8, comparing removal of the  $\pi^{\text{th}}$  mode versus preserving the symmetric structure of the matrix. As with the diagonal norm, forcing removal of the  $\pi^{\text{th}}$  mode leads to much larger amplitude overshoots at the endpoints. This contributes to a transient growth mode, as the leading singular value ranges from  $\sigma_1 = 1.01944896$  at  $N = 9$  and asymptoting to  $\sigma_1 = 1.01781687$  for large  $N$ . When

## 4.2 Energy and Entropy Stability

It is often desirable for the underlying numerical schemes to contribute some degree of energy or entropy stability for simulating the desired system. The intent of the filter is to augment that stability by

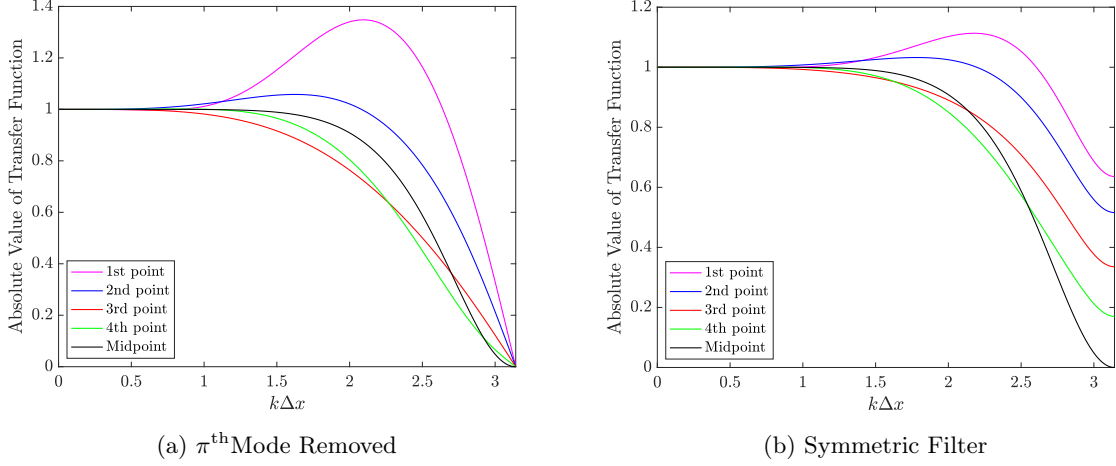


Figure 8: Effect of removing the  $\pi^{\text{th}}$  mode near the boundaries of a Padé-type filter with  $N = 33$ .

helping to prevent non-physical over/undershoots and providing a dealiasing effect for non-linear terms. The semi-discrete energy stability of a scalar system may be expressed as,

$$\mathbf{u}^T \mathcal{P} \frac{d\mathbf{u}}{dt} = \frac{dE}{dt} \leq 0 \quad (18)$$

where  $E = \frac{1}{2} \mathbf{u}^T \mathcal{P} \mathbf{u}$ . Hence, the leading singular value of  $\mathcal{R} \mathcal{F} \mathcal{R}^{-1}$  is a direct measure of the energy stability. If  $\sigma_1 \leq 1$ , then the filter can be regarded as provably dissipative, whereas  $\sigma_1 > 1$  suggests a destabilizing effect.

The mathematical analyses thus far have considered filter behaviors primarily in the context of scalar equations. Nevertheless, fluid-dynamic systems are vector equations requiring a matrix integration norm to meaningfully evaluating the magnitude of a solution perturbation. A prominent norm is that of Chu[13], which defines the total disturbance energy as,

$$E = \frac{1}{2} \int \left( \frac{R\bar{T}\rho'^2}{\bar{\rho}} + \bar{\rho}u'_i u'_i + \frac{\bar{\rho}C_v T'^2}{\bar{T}} \right) dV \quad (19)$$

where the prime denotes a perturbation from the reference condition denoted by the overbar. Accordingly, the contribution from each point may be written as,

$$dE = q'^T \mathcal{M} q' \quad (20)$$

where  $q'$  contains the primitive variables  $\rho$ ,  $u_i$ ,  $T$ , and the weighting matrix  $\mathcal{M}$  is

$$\mathcal{M} = \text{diag} \left[ \frac{R\bar{T}}{\bar{\rho}}, \bar{\rho}, \bar{\rho}, \bar{\rho}, \frac{\bar{\rho}C_v}{\bar{T}} \right] J^{-1} \quad (21)$$

where  $J^{-1}$  is the inverse of the local curvilinear transformation Jacobian (i.e., the local volume). It was recently shown by Vogel and Coder[14] that a total disturbance entropy can be calculated using the Chu weighting matrix divided by reference temperature. Because  $\mathcal{M}$  is diagonal, the singular values of the vector filter are identical to those of the scalar filter. Thus, filtering the primitive variable set  $[\rho, u, v, w, T]$  offers provable energy and entropy stability to Navier-Stokes simulations.

Other variable sets may be used with the Chu norm and/or Vogel-Coder norm by including the Jacobian relating them to the above-defined set of primitive variables. In other words,

$$dE = w'^T q_w'^T \mathcal{M} q_w w' \quad (22)$$

The transient growth behavior of the filter then becomes dependent on  $q_w$  (i.e., how dense the matrix is), the specific distribution of volumes  $J^{-1}$ , and whether or not the reference condition is uniform in space. Therefore, generalized statements about the matrix-norm transient growth for an arbitrary variable set may not be possible.

## 5 Test Cases

### 5.1 One-Dimensional Linear Advection

The first test case considered is linear advection diffusion,

$$\frac{\partial u}{\partial t} + a \frac{\partial u}{\partial x} = 0 \quad (23)$$

on  $x = [0, 1]$ . The domain is taken to be periodic; however, the periodicity is imposed by imposing the rightmost value from the domain interior as the target value on the boundaries at both  $x = 0$  and  $x = 1$ .

For this study, the advection speed is taken to be  $a = 1$  (right-moving), and the initial condition is a Gaussian bump,

$$u(x, 0) = \exp \left[ - \left( \frac{10}{\Delta x} \right) \left( x - \frac{1}{2} \right)^2 \right] \quad (24)$$

Two different sets of simulations were considered. Grid spacing of  $\Delta x = 0.02$  is used, and the equation is integrated using a 4<sup>th</sup>-order Runge-Kutta method with CFL condition of 0.5. The first set employs the 4<sup>th</sup>-order bandwidth-optimized SBP scheme with diagonal  $\mathcal{P}$  described by Coder [11]. Three different variations were considered: unfiltered, use of an inconsistent 8<sup>th</sup>-order filter that removes the  $\pi^{\text{th}}$  mode, and a fully consistent, symmetric 8<sup>th</sup>-order filter. The filters are applied after every global time step (as opposed to after every stage). The resulting waveforms after 20 periods are shown in Fig. 9. All three solutions share a similar peak amplitude of the waveform, but the oscillatory behavior around the peak differs significantly. The unfiltered result has a strong oscillation through the domain. The asymmetric filter damps the oscillations trailing the waveform, but seems to excite the leading oscillations, as it has higher amplitude than the unfiltered result. The symmetric filter damped the trailing oscillations, and improved over the unfiltered result ahead of the waveform. The respective  $L^2$ -norms of the errors are 0.9666 for the unfiltered results, 1.1277 with the asymmetric filter, and 0.8086 with the symmetric filter. Further insight may be gained by comparing the relative spectral content of the initial and final waveforms, as shown in Fig. 10. The two filters damp the poorly resolved content at higher wavenumbers; however, it is observed that the asymmetric filter has a backscatter effect where the energy content at lower wavenumbers slightly increased through the simulation. This is consistent with the notion of transient growth implied by non-orthogonality of the eigenvectors.

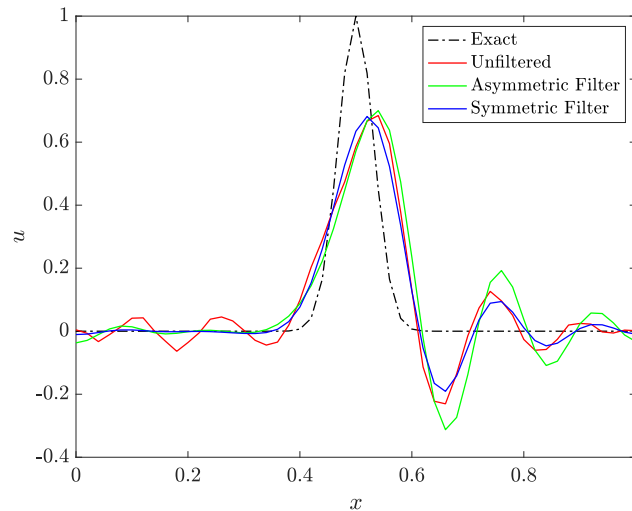


Figure 9: Waveform comparison of linear advection of Gaussian bump after 20 periods for diagonal  $\mathcal{P}$ .

The second set of simulations employ a pentadiagonal, 4<sup>th</sup>-order accurate Padé scheme with 3<sup>rd</sup>-order summation-by-parts boundary closure [11]. A comparison of the results for unfiltered, asymmetrically filtered, and symmetrically filtered solutions show the same trends as the case with a diagonal  $\mathcal{P}$ . The unfiltered result has additional oscillations throughout the domain, and application of an asymmetric filter that fully removes the  $\pi^{\text{th}}$  mode increases the oscillations upstream of the wave. The symmetric filter shows generally improved behavior. The  $L^2$ -norms of the errors are 0.8462 for the unfiltered results,

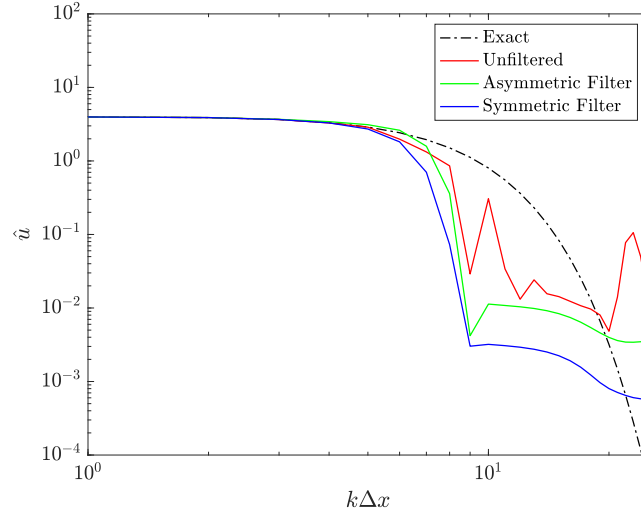


Figure 10: Spectral content comparison of linear advection of Gaussian bump after 20 periods for diagonal  $\mathcal{P}$ .

0.8652 with the asymmetric filter, and 0.7058 with the symmetric filter. As with the diagonal scheme, the asymmetric filter shows a backscatter effect at lower wavenumbers.

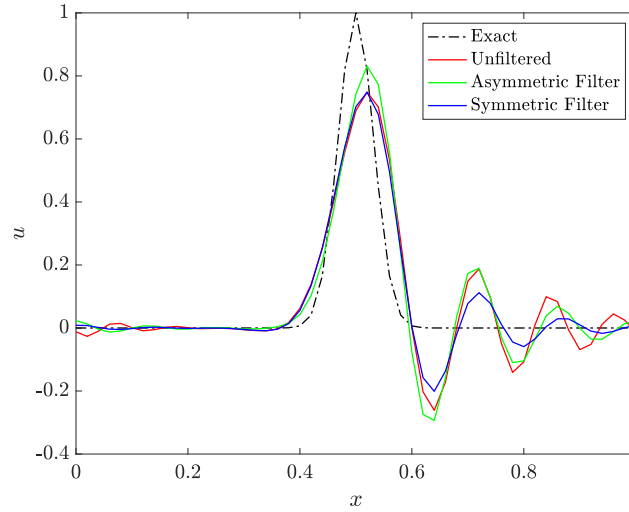


Figure 11: Waveform comparison of linear advection of Gaussian bump after 20 periods for pentadiagonal  $\mathcal{P}$ .

## 5.2 2D Inviscid Homogeneous, Isotropic Turbulence

The second test case considered is the inviscid advection of 2D, homogenous, isotropic turbulence at incompressible conditions. For these simulations, a vorticity-based formulation is used, i.e.

$$\frac{\partial \omega}{\partial t} + u \frac{\partial \omega}{\partial x} + v \frac{\partial \omega}{\partial y} = 0 \quad (25)$$

This equation is solved on a uniform grid with  $x = [-\pi, \pi]$  and  $y = [-\pi, \pi]$ , each 129 points (endpoints inclusive). The residual is evaluated in a non-conservative form, with the derivatives of  $\omega$  calculated using a finite-difference scheme, and the velocities determined from  $\omega$  using fast Fourier transforms. To exercise the influence of boundary contributions, a background velocity of  $u_\infty = 1$  is added as the constant of integration. Periodic boundaries are used with the boundary fluxes specified to the arithmetic

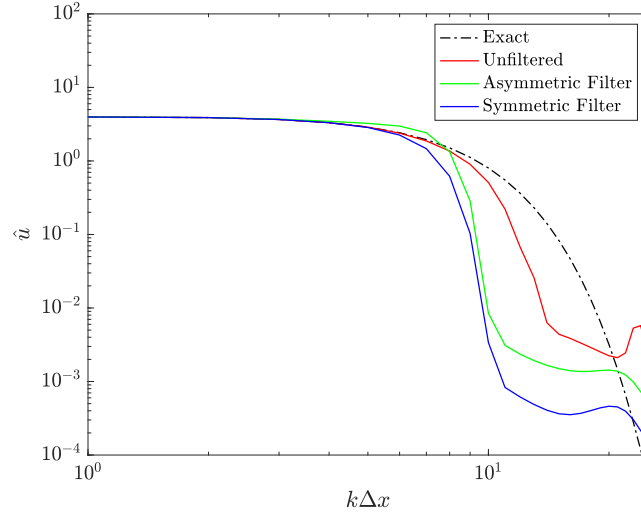


Figure 12: Spectral content comparison of linear advection of Gaussian bump after 20 periods for pentadiagonal  $\mathcal{P}$ .

average of the end-point fluxes (i.e., centrally differenced). The initial condition is generated as a random distribution of random-strength Taylor-type vortices based on the work of Ref. [15]. The same initial condition is used for all simulations, and is plotted in Fig.

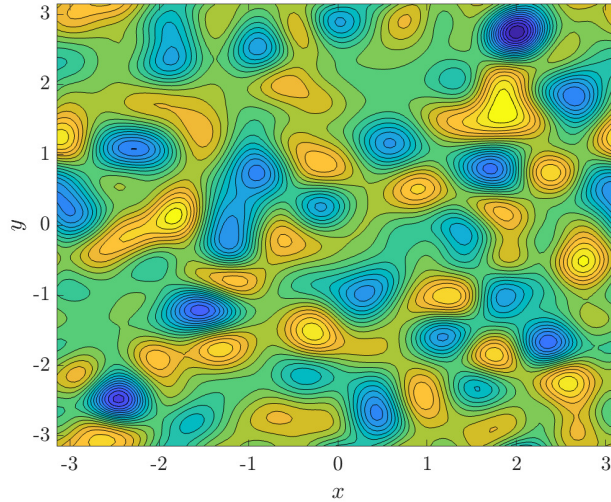


Figure 13: Initial condition on  $\omega$  for inviscid HIT.

The nonlinearities and chaotic dynamics of the advection terms provide a practical test of the differencing scheme and filters. As an inviscid, incompressible formulation, the integrated kinetic energy in the domain should be exactly preserved, thus providing a quantitative metric for evaluating the filters. Results are shown in Fig. 14 for the total kinetic energy predicted by the 4<sup>th</sup>-order explicit and 4<sup>th</sup>-order Padé scheme with pentadiagonal schemes with asymmetric and symmetric filters. With the diagonal-norm scheme, both filters show similar qualitative behaviors, but the symmetric filter preserves the kinetic energy better over the course of the simulation. For the pentadiagonal norm, the asymmetric filter is poorly behaved, showing erratic response in the kinetic energy. The symmetric filter is overall better behaved and is closer to the desired monotonic behavior. Note that neither symmetric filter showed perfectly dissipative kinetic energy, but this is a side-effect of using a vorticity formulation rather than a velocity formulation to the equations. To confirm this, the time history of integrated enstrophy,  $\mathcal{E} = \iint \omega^2 dA$ , for the diagonal-norm schemes was interrogated and the results are shown in Fig. 15. Both the symmetric and asymmetric filters show very similar response over the course of the simulation.

With a symmetric filter, the enstrophy decay is fully monotonic, whereas with the asymmetric filter, there is a slight increase in enstrophy around  $t = 0.05$ . While small and ultimately inconsequential for this simulation, it does confirm a slight instability when the  $\pi^{\text{th}}$  mode is forced to be removed.

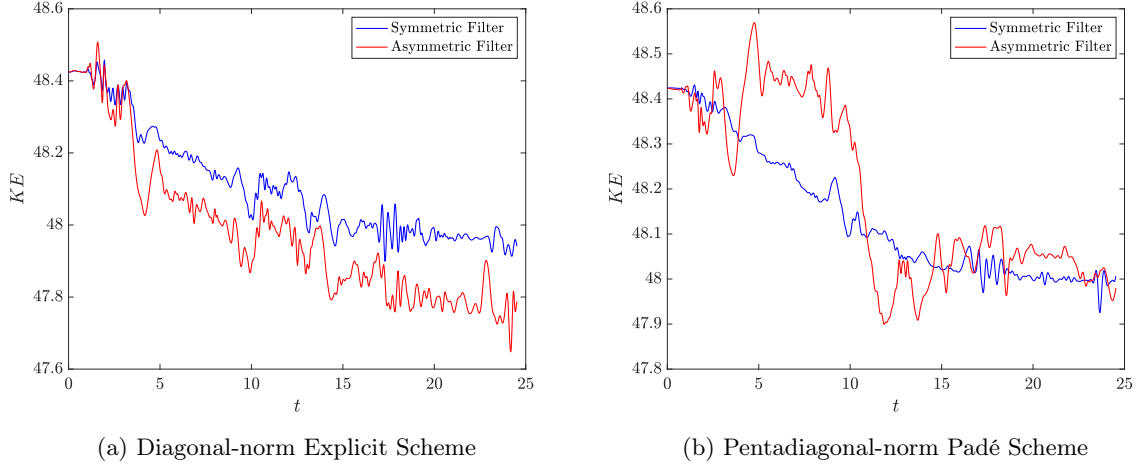


Figure 14: Evolution of integrated kinetic energy for inviscid, homogeneous isotropic turbulence.

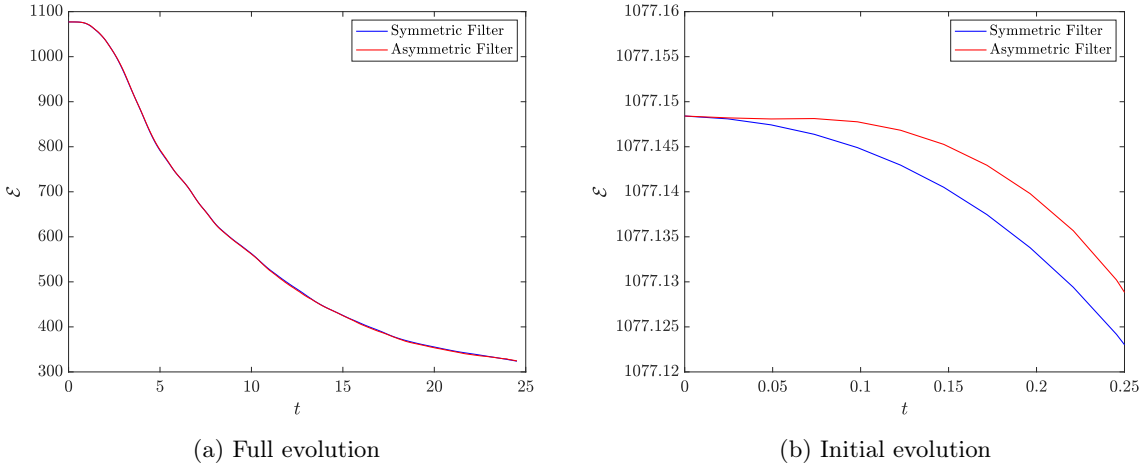


Figure 15: Evolution of enstrophy from diagonal-norm schemes.

The final states from the various simulations are shown in Figs. 16 and 17, and energy spectra are plotted in Fig. 18. Visually, there is not an appreciable difference in the turbulence content whether a symmetric or an asymmetric filter is used, and this is supported quantitatively by the energy spectra. All schemes show similar distributions up until the highest wavenumbers, which is where the filters are most active. The backscatter that was observed for the linear advection case was not observed, and this is presumably because the vorticity equation is nonlinear and naturally transfers energy from lower to higher wavenumbers.

## 6 Conclusion

High-order, finite-domain filters were investigated in the context of turbulent flow simulations. Although the interior filter stencils are calibrated based on Fourier analysis, such an analysis is not appropriate near the domain boundaries due to the lack of periodicity. Instead, it is more appropriate to use matrix analyses to understand the transfer function (it is worth noting that in the limit of an infinite/periodic domain, the matrix eigenvalues equal to Fourier eigenvalues). It was observed that many filters calibrate their stencils near the boundaries to remove the  $\pi^{\text{th}}$  mode based on Fourier analysis. When considered with respect to the integration norms of the underlying finite-difference or finite-volume scheme,

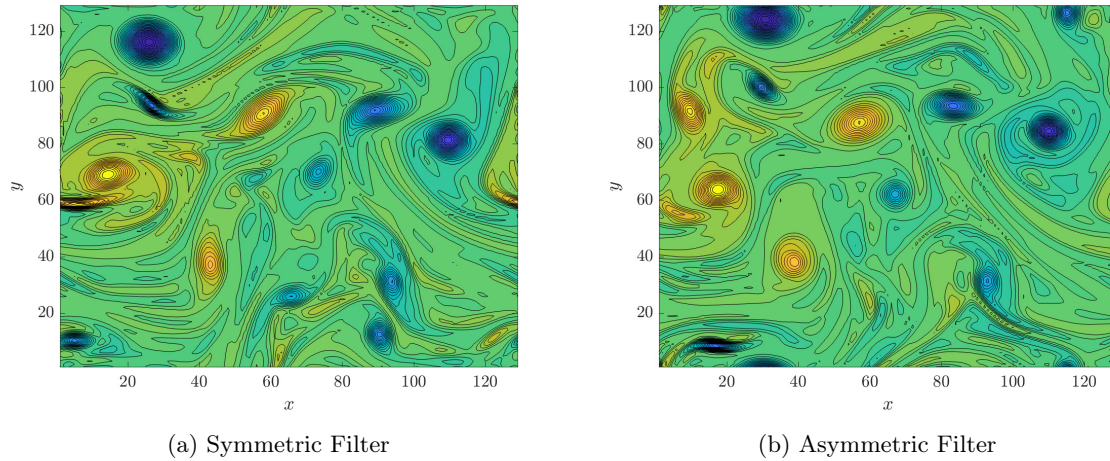


Figure 16: Final HIT states obtained with the diagonal-norm scheme.

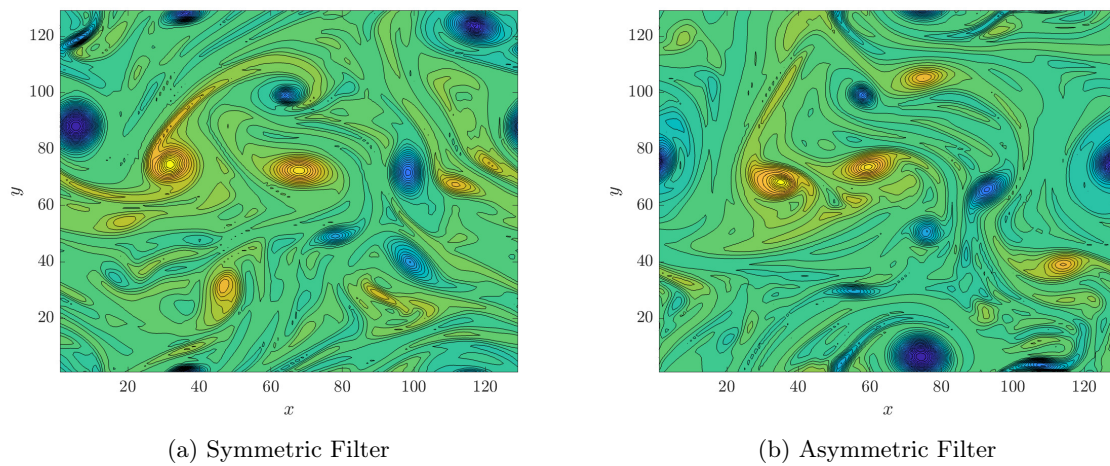


Figure 17: Final HIT states obtained with the pentadiagonal-norm scheme.

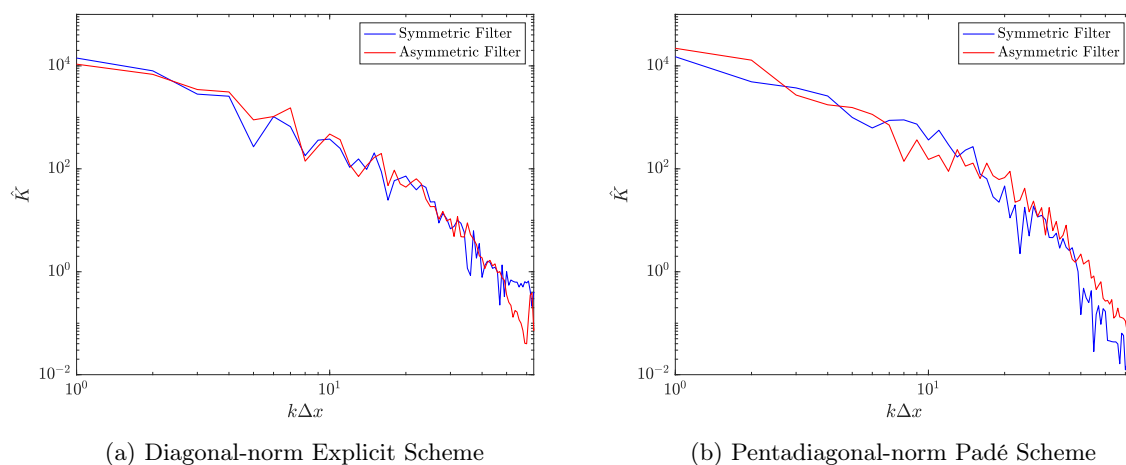


Figure 18: Energy spectra of the final HIT states.

inconsistency occurs which leads to the filter matrix being generally non-symmetric. This leads to non-orthogonal eigenvectors, which permits transient growth of solution content through filter application, despite having a contractive eigenvalue spectrum.

Behaviors of bespoke finite-domain filters for two different summation-by-parts finite-difference schemes were analyzed, one with a diagonal norm, and one Padé scheme with pentadiagonal norm. For both differencing schemes, an inconsistent filter that forces removal of the  $\pi^{\text{th}}$  mode at boundaries and a consistent, symmetric filter were used. When tested with the linear advection of a Gaussian bump, the symmetric filters outperformed the asymmetric filters in final solution accuracy. Moreover, the asymmetric filters were found to induce some backscatter of content to lower wavenumbers.

Application of the schemes and filters to advection of two-dimensional, inviscid, incompressible turbulence confirms improved behavior of symmetric filters versus forcing removal of the  $\pi^{\text{th}}$  mode at boundaries. The symmetric filters showed better preservation of the kinetic energy through the simulation, despite the use of a vorticity formulation. Monotonic decay of enstrophy was confirmed for the symmetric filter. The asymmetric filter showed a slight growth in the initial stages of the simulation, but the long-time behavior was consistent with the symmetric filter.

Overall, it is recommended that filters be constructed so that they are consistent and symmetric with respect to the norm of the underlying numerical scheme. This may require forgoing removal of the  $\pi^{\text{th}}$  mode at boundaries, but as discussed above, the argument for doing so is contradictory to having a finite domain.

## References

- [1] Sanjiva K. Lele. Compact finite difference schemes with spectral-like resolution. *Journal of Computational Physics*, 103:16–42, 1992.
- [2] Miguel R. Visbal and Datta V. Gaitonde. On the use of higher-order finite-difference schemes on curvilinear and deforming meshes. *Journal of Computational Physics*, 181:155–185, 2002.
- [3] Antony Jameson. Origins and further development of the jameson–schmidt–turkel scheme. *AIAA Journal*, 55(5), 2017.
- [4] Thomas H. Pulliam. Artificial dissipation models for the euler equations. *AIAA Journal*, 24(12), 1986.
- [5] Thomas Pulliam. High order accurate finite-difference methods: As seen in overflow. *20th AIAA Computational Fluid Dynamics Conference*, AIAA Paper 2011–3851, Honolulu, HI, June 2011.
- [6] Xu-Dong Liu, Stanley Osher, and Tony Chan. Weighted essentially non-oscillatory schemes. *Journal of Computational Physics*, 115(1):200–212, 1994.
- [7] Daniel J. Garmann. *Characterization of the vortex formation and evolution about a revolving wing using high-fidelity simulation*. PhD thesis, University of Cincinnati, 2013.
- [8] Ardeshir Hanifi, Peter J. Schmid, and Dan S. Henningson. Transient growth in compressible boundary layer flow. *Physics of Fluids*, 8(3):826–837, 1996.
- [9] Tomas Lundquist and Jan Nordström. Stable and accurate filtering procedures. *Journal of Scientific Computing*, 82(16):15–35, 2020.
- [10] David A. Craig Penner and David W. Zingg. High-order artificial dissipation operators possessing the summation-by-parts property. *2018 AIAA Aviation Forum*, AIAA Paper 2018–4165, Atlanta, GA, June 2018.
- [11] James G. Coder. Bandwidth-optimized summation-by-parts operators for high-resolution turbulent flow simulations. *2023 AIAA Aviation Forum*, AIAA Paper 2023–3862, San Diego, CA, June 2023.
- [12] Ayaboe K. Edoh and David C. Del Rey Fernandez. Padé summation-by-parts operators for spectral resolvability on bounded domains: The first derivative. *2019 AIAA Aviation Forum*, AIAA Paper 2019–3203, Dallas, TX, June 2019.
- [13] B.-T. Chu. On the energy transfer to small disturbances in fluid flow (part i). *Acta Mechanica*, 1(3):215–234, 1965.
- [14] Ethan A. Vogel and James G. Coder. A novel entropy normalization scheme for characterization of highly compressible flows. *Theoretical and Computational Fluid Dynamics*, 36(4):641–670, 2022.
- [15] K. Taira, A. G. Nair, and S. L. Brunton. Network structure of two-dimensional decaying isotropic turbulence. *Journal of Fluid Mechanics*, 795, R2, 2016.